Engineering Transactions, **71**(3): 399–417, 2023, doi: 10.24423/EngTrans.2453.20230704
Institute of Fundamental Technological Research Polish Academy of Sciences (IPPT PAN)
Université de Lorraine • Poznan University of Technology

Research Paper

Influence of Cutting Parameters and Tool Edge Geometries on the Machinability of AISI 52100 Steel in Hard Whirling

Shuquan SONG[1),2)*], Yu ZHANG[1)], Jiangtao CHENG[1)], Hao ZHANG[1)], Xiangyu GUAN[1)], Dunwen ZUO[3)], Xiaoqiang SHEN[4)]

[1)] *School of Mechanical Engineering, Yancheng Institute of Technology*
Yancheng 224051, China

[2)] *Zhejiang Provincial Key Laboratory for Cutting Tools, Taizhou University*
Taizhou 318000, China

[3)] *College of Mechanical and Electrical Engineering*
Nanjing University of Aeronautics & Astronautics
Nanjing, 210016, China

[4)] *Department of Precision Manufacturing Engineering*
Suzhou Vocational Institute of Industrial Technology
Suzhou, 215104, China

*Corresponding Author e-mail: ssq@ycit.edu.cn

The synergistic effect of prepared tool edge and cutting parameters in hard whirling is still unclear, limiting its application in producing large precision ball screws. This paper aims to reveal the effect mechanism of cutting parameters and edge geometries in the whirling process to improve the stability of ball screw quality. A novel cutting force measurement strategy is proposed, and a systematic study of cutting force, surface quality and tool wear is implemented. The results show that small feed (less than 0.15 mm) and high cutting speed (more than 180 m/min) can ensure machining efficiency and improve surface quality. The machining quality can be improved when the edge radius is 10 μm, and the chamfer size is 0.1 mm × 20°. The tool with a 30 μm edge radius has a low probability of early failure, but the later wear is severe and timely sharpening is recommended. This study could guide cutting parameters and edge geometry optimization to improve the stability of the quality in hard whirling.

Keywords: hard whirling; cutting edge radius; cutting parameters; machinability.

1. Introduction

As the core mechanical element in the ball screw transmission, the threaded raceway plays a crucial role in realizing the function of the screw and is difficult to machine. Hard whirling can employ super-hard tools to perform hard cutting of ball screws, meeting high efficiency and green environmental protection re-

quirements. It has the advantages of low cutting force and high material removal rate, which is especially suitable for processing large precision ball screws and has gradually become its primary processing method [1, 2].

The relative motion between the tool and the part in whirling is complex, and many factors impact the machining process and the quality. Son *et al.* [3] developed an undeformed chip thickness model and investigated the cutting forces in whirling using simulation methods. Studies have shown that due to the effects of bottom and side edges, the principal cutting force and passive force were relatively larger than the feed force. Lee *et al.* [4] studied the overcutting problem of planetary milling and side milling comparatively using geometric methods, and investigated the variation law of cutting force in whirling experimentally. They found that the cutting force of side milling is less than half of that in planetary milling under the same feed. Side milling is superior to planetary milling for the described factors, such as threading time, cumulative lead, and profile errors. A study by Liu *et al.* [5] showed that the maximum depth of cut greatly influences surface topography, while the cutting velocity and maximum depth of cut significantly affect workpiece temperature. He *et al.* [6] proposed a transient thermal analytical model to analyze the temperature distribution in the cutting area for screw whirling. They concluded that the investigation shows that the influence of the un-deformed chip thickness on the maximum temperature distribution of the cutting area is more than the influence of the un-deformed chip width and the un-deformed chip cross-section area. The chip temperature is mainly caused by the shear plane heat source in the lead-screw whirling milling. Guo *et al.* [7, 8] systematically investigated the residual stresses, nano-hardness, surface roughness and other integrity indexes on the machined raceway surface in hard whirling. They concluded that the maximum temperature of the machined surface exceeded the phase transition temperature, which caused the transition from γ-Fe to α-Fe, resulting in residual compressive stresses on the machined surface, and the magnitude of the compressive stress values was related to the α-Fe content. Liu *et al.* [9] developed an analytical model to predict workpiece residual stresses in whirling by correlating the effect of surface topography. The results showed that the compressive residual stress of the workpiece surface at the highest point is higher than that at the lowest point of the surface topography. Using response surface methodology, Guo *et al.* [10] investigated the effect of cutting parameters on surface roughness and cutting forces. They found that the minimization of tangential cutting forces and surface roughness could be obtained by selecting the optimized cutting parameters. Liu *et al.* [11] proposed two kinds of machine learning methods to predict the residual properties of the ball screw raceway in whirling. Wang *et al.* [12] developed a dynamic model of whirling considering the multi-point variable constraints induced by floating supports and clamping devices, and effectively analyzed the dynamic

performance of a large lead screw. He *et al.* [13] presented an analytical model for predicting the specific cutting energy in whirling. The results show that the analytical model can effectively predict the specific cutting energy (SCE), and the effects of cutting parameters and material removal rate on SCE were investigated.

The intermittent cutting characteristics of hard whirling and the high hardness of the workpiece material make PCBN (polycrystalline cubic boron nitride) tools prone to early failure [14], and this abnormal wear seriously affects the consistency of the middle diameter of the ball screw and the accuracy of the raceway. Edge preparation can effectively remove microscopic defects of the cutting edge, reduce early tool failure and prolong tool life [15], which is widely used in the fabrication of hard whirling tools. The edge geometry of a prepared tool edge can have a profound effect on the machining process. Wu *et al.* [16] investigated cutting edge radius and material grain size effects on cutting forces. The results showed that the impact of cutting edge radius on cutting force and specific cutting energy was more significant than the effect of material grain size. Ventura *et al.* [17] studied the machinability of hardened AISI 4140 steel in turning with various tool microgeometries. The results showed that cutting edge microgeometry affects mainly the feed and passive force components. Klocke *et al.* [18] studied the turning of hardened steel with PCBN tools and proposed an edge design solution for high performance tools, which was tested and proved to significantly extend tool life by 30% while improving material removal rate and workpiece surface quality. Rech *et al.* [19] investigated the effect of edge radius on the wear resistance of powder metallurgical HSS tools experimentally. It was found that using the abrasive flow preparation method, tools with an edge radius of 10 μm had the longest service life that was 4–5 times longer than that of the unprepared tools. Endres *et al.* [20] studied the effect of the corner and edge radii on flank wear and experimentally investigated the optimal edge radius for turning tools with specific parameters.

To improve the stability of machining quality, this paper designs and conducts a series of hard whirling tests to investigate the effects of cutting speed, feed rate and tool edge parameters on cutting force, surface quality and tool wear in the hard whirling of large ball screws. To address this, we propose a toolholder-type force measurement method for hard whirling, using an infrared thermometer to obtain the cutting temperature, and measuring the tool wear as well as the quality of the workpiece after machining. This study can provide a basis for process parameter optimization and tool structure design.

2. Materials and methods

Hard whirling is a high-speed machining process that progressively envelops the screw raceway with multiple forming tools mounted on an eccentric cutter

head. The workpiece speed is low, the cutter speed is high, and the cutter feeds one lead per revolution of the workpiece, thus machining the ball screw. The scheme of hard whirling of the ball screw is shown in Fig. 1, where e is the eccentricity of the cutterhead and the workpiece, n_c is the speed of the tool, n_w is the speed of the workpiece, o_c is the tool's center of rotation, and o_w is the workpiece's center of rotation. With high precision, high efficiency, low cost and environmental friendliness, hard whirling is gradually replacing the traditional profile grinding process and becoming the mainstream technology for large precision ball screw machining.

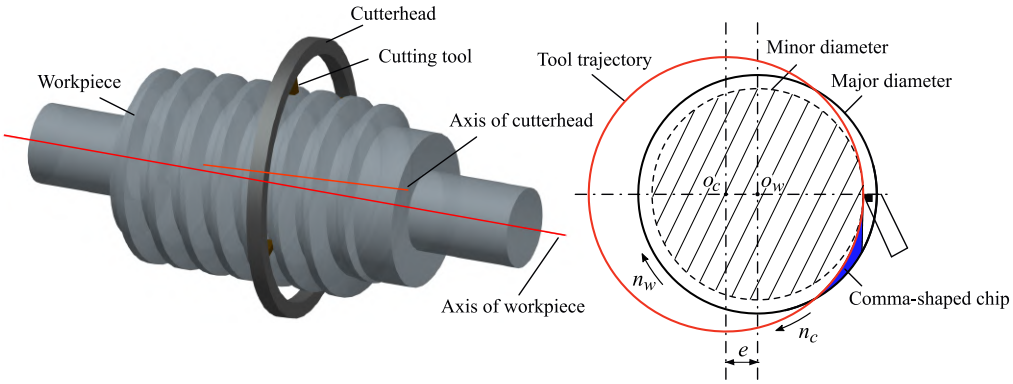

FIG. 1. The scheme of hard whirling of the ball screw.

2.1. Machining experiment

2.1.1. Experimental procedure. The workpiece is a hardened and ground AISI 52100 bar stock, the material properties of AISI 52100 are shown in Table 1. The outside diameter of the workpiece is 79.4 mm, the length is 3400 mm, the screw helix angle is $2°17'$, and the pitch is 10 mm. Five groups of tools with different cutting edge parameters were used for cutting in the experiment. Each group has three tools of the same size, mounted evenly on the circumference of the cutter head. Each group of tools was tested for cutting with 16 different machining parameters. After cutting 20 mm for each machining parameter, the tool was axially fed 10 mm with idle stroke before the next cut. A total of 5 groups of tools with different specifications were employed for the test. After each

Table 1. Material properties of AISI 52100 [21, 22].

Young's modulus [GPa]	Poisson's ratio	Ultimate tensile strength [MPa]	Yield strength [MPa]	Density [kg/m^3]	Hardness [HRC]
201	0.28	1640	1230	7827	62

group of tools was cut 16 times according to different machining parameters, the cutter was axially fed 30 mm, and another group of tools was replaced for the cutting test. The cutting test scheme and actual machining result are shown in Fig. 2.

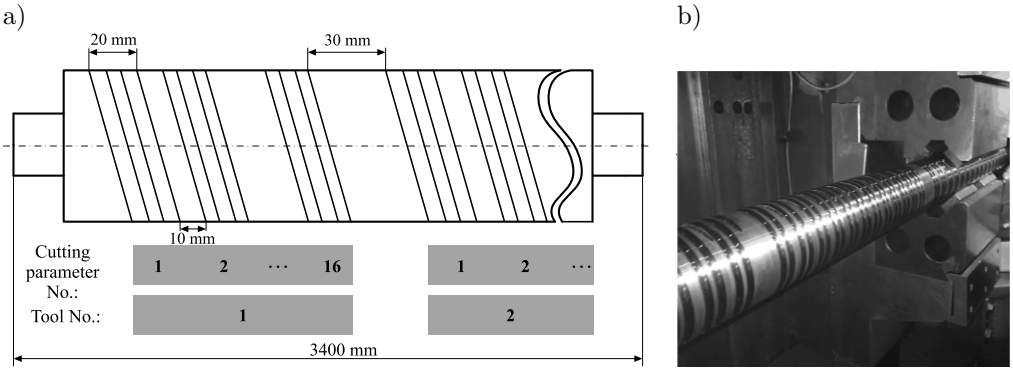

FIG. 2. Cutting experiment procedure: a) experimental design of hard whirling, b) on-site machining result.

2.1.2. Machine tool and cutting tool. The machining test was carried out with HJ092 × 80 CNC hard whirling machine tool. The shape and geometric dimensions of the PCBN tool are shown in Fig. 3. The tool is welded by the cemented carbide substrate and the PCBN insert. The rake angle of the tool is 0°, the relief angle is 7°. Five groups of tools with different edge parameters shown in Table 1 were used. The PCBN tool material grade is PNC108. It is

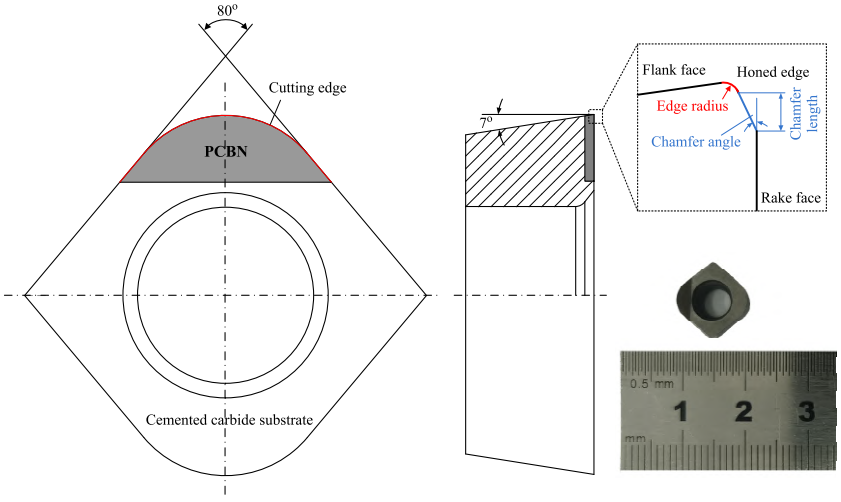

FIG. 3. Profile and geometric parameters of the tool.

made of ultra-fine cubic boron nitride and cermet bonding agent sintered by high temperature and pressure, where the cermet bonding agent is mainly titanium nitride and a small amount of aluminum nitride. The tool edge parameters are shown in Table 2, and tool material parameters are shown in Table 3.

Table 2. Tool edge parameters.

Tool number	Chamfering parameters		Edge radius [μm]
	Length [mm]	Angle [°]	
Tool 1	0.1	20	10
Tool 2	0.1	20	20
Tool 3	0.15	25	10
Tool 4	0.1	20	30
Tool 5	0.15	25	30

Table 3. Tool material parameters.

Material type	CBN content [Vol%]	Particle size of CBN [μm]	Binder
PNC108	50	1	TiN/AlN

2.2. Cutting force measurement and data processing

The available space on the whirling cutter head is small, and there is not enough space for the dynamometer to be installed. In addition, as the cutter head and workpiece rotate in hard whirling, the signal transmission line is easily tangled. The collected force measurement signal must be output through an intermediary that does not follow the tool rotation. As shown in Fig. 4, a toolholder-type whirling force measurement device was designed for this study. A small three-way force sensor, Kistler 9602A3, was mounted in the groove under the insert. The cutting force applied to the tool was transmitted to the force sensor through the backing plate, and the electrical slip ring was used to output the charge signal to the computer. The cutting force sensor was mounted underneath the tool, and the workpiece was clamped with a chuck and center.

Due to the intermittent cutting process of the single tool in hard whirling, the measured cutting forces are intermittently valid. The measured cutting forces must be post-processed to eliminate the effect of zero-line drift and obtain the measured data more accurately. In the stable cutting stage, five consecutive sets of valid data areas are taken, and each valid data area corresponds to one single-edge cutting cycle. In a single cutting cycle, the average and peak cutting forces are calculated, and the actual average and peak cutting forces of a single cutting cycle are obtained by subtracting the minimum cutting force in the area, and

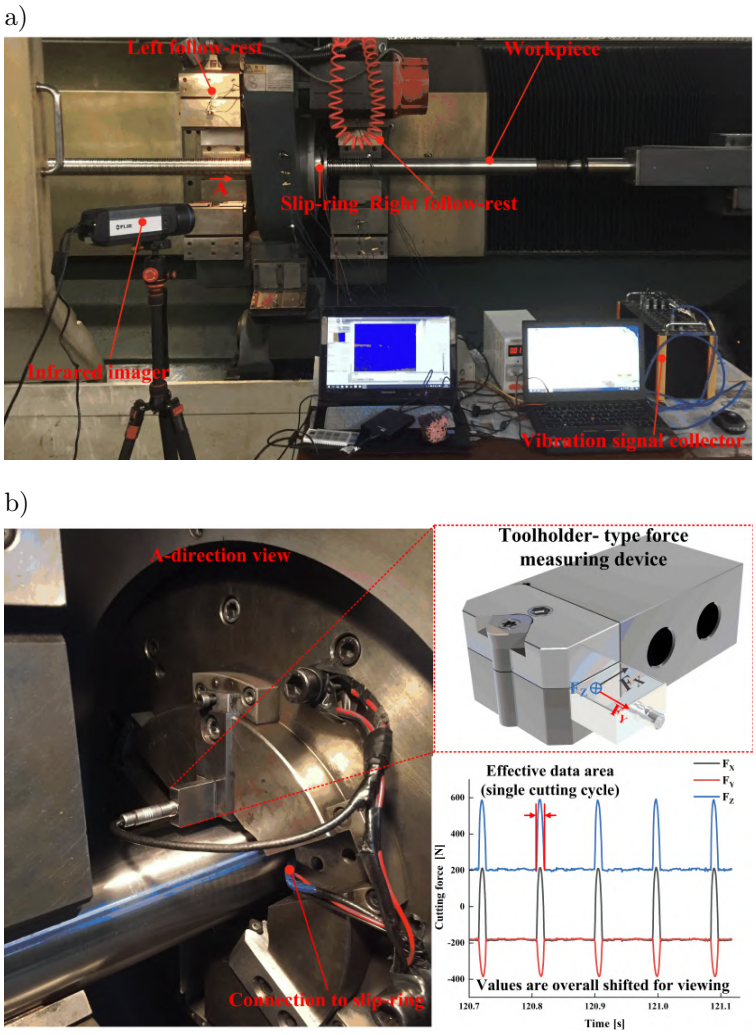

FIG. 4. Experimental setup of hard whirling and toolholder-type force measuring device:
a) experimental setup for hard whirling,
b) cutting force measuring device and its measuring signal.

then the arithmetic mean of the five sets of data is taken as the final cutting force value.

2.3. The surface quality of the workpiece and tool wear

To study the distribution of residual stress and surface roughness of large ball screws, we analyze the influence of process and tool edge parameters on the quality of the machined surface. It will help find the optimized combination

of process and tool parameters. The machined screw was cut into several segments using a wire-cutting process, and the residual stress and roughness were measured, respectively. The residual stress measurement was performed by the X-ray diffraction method. In this study, the roughness of the screw surface is characterized by surface roughness Ra. Ra represents the arithmetic mean of the absolute value of the distance from each point on the measured contour to the contour's centerline within the sampling length, and the larger the Ra value, the rougher the surface. Ra can objectively reflect the geometric characteristics of the measured contour. The surface roughness Ra was measured by the Hommel-Etamic T8000 RC contact roughness profiler. As shown in Fig. 5, the residual stress measuring points A, B and C are distributed according to the feed direction. The raceway roughness was measured in the left, middle and right sections according to the feed direction.

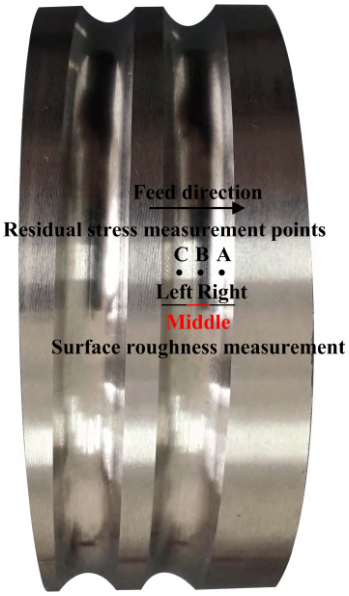

FIG. 5. Schematic diagram of the measurement locations of residual stresses and surface roughness in the screw fragment.

We have also carried out experimental studies on tool wear. In the experiment, every 50 m cutting length interval, the tool flank wear was observed with an XJP-6A tool microscope and the maximum wear was measured with the Digimizer software. Chip micromorphology and tool wear were also observed using an FEI Nova NanoSEM 450 scanning electron microscope. Energy dispersive spectroscopy (EDS) analyses were performed using an AZtec X-MaxN80 energy spectrometer to investigate tool wear patterns.

3. Results and discussion

3.1. Effect of cutting parameters on cutting forces and surface quality

As shown in Fig. 6, as the feed per tooth increases, the radial force, feed force and principal cutting force tend to increase. Since the increase in feed per tooth makes the shear area of the first deformation zone increase with the other parameters unchanged, which increases the energy required to remove the material, there is a more significant increase in all three components of the cutting force. Among them, when the cutting speed was 160 m/min and the feed per tooth was increased from 0.1 mm to 0.4 mm, the mean values of radial force, feed force and principal cutting force increased to 68.37%, 43.76%, and 126.63%, respectively. The cutting thickness is small at small feeds (0.1 mm, 0.15 mm). Due to the existence of the honed edge and the negative chamfering, the radial force is greater than the principal cutting force and feed force. This may be attributed to the fact that the negative chamfer of the tool edge is equivalent to the actual rare face when cutting, and the tool has a significant pushing and squeezing effect on the workpiece in addition to the shearing effect. When the feed is larger (0.25 mm, 0.4 mm), the cutting thickness increases, the pushing

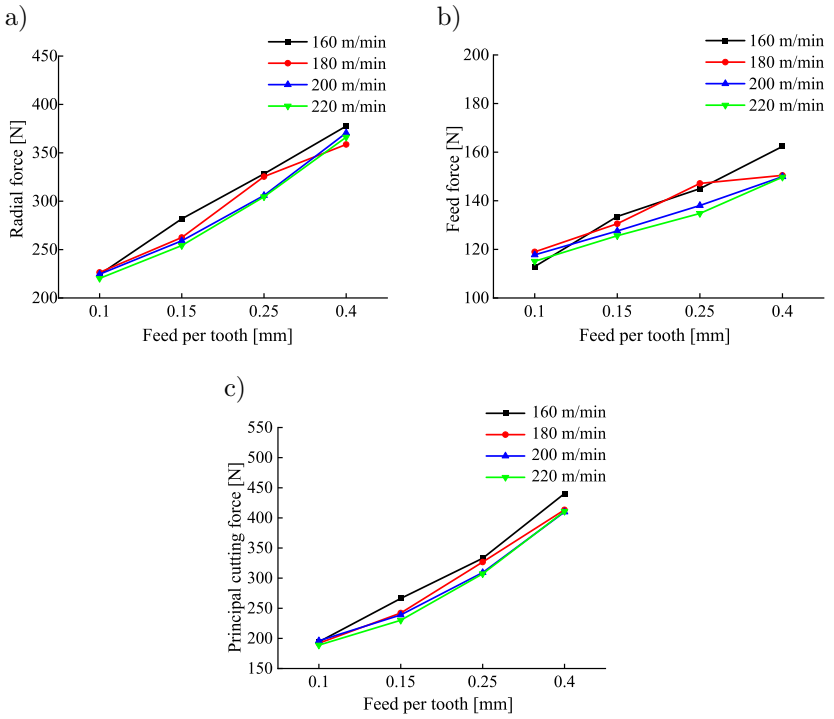

Fig. 6. The effect of cutting parameters on cutting forces (tool 2): a) radial force, b) feed force, c) principal cutting force.

and squeezing effect of the cutting edge on the workpiece is weakened, and the principal cutting force gradually exceeds the radial force. The increased cutting speed decreases the friction coefficient between the tool and chip, the chip deformation coefficient decreases, and the cutting force decreases with increased cutting speed [23, 24]. However, relative to the feed per tooth, the cutting force does not change much as the cutting speed changes, and the effect of cutting speed on cutting force is insignificant.

Figure 7a shows the variation of residual stress on the workpiece surface with the cutting speed when cutting with tool 2 ($f_z = 0.25$ mm, point B). It can be seen from the figure that there are residual compressive stresses on the surface of the workpiece under different cutting speeds in hard whirling. When the cutting speed increases, the residual stress on the surface of the workpiece shows a trend of decreasing and then increasing. When the cutting speed is 160 m/min, the surface residual compressive stress obtains the maximum value of 368 MPa, and when the cutting speed is 200 m/min, the surface residual compressive stress

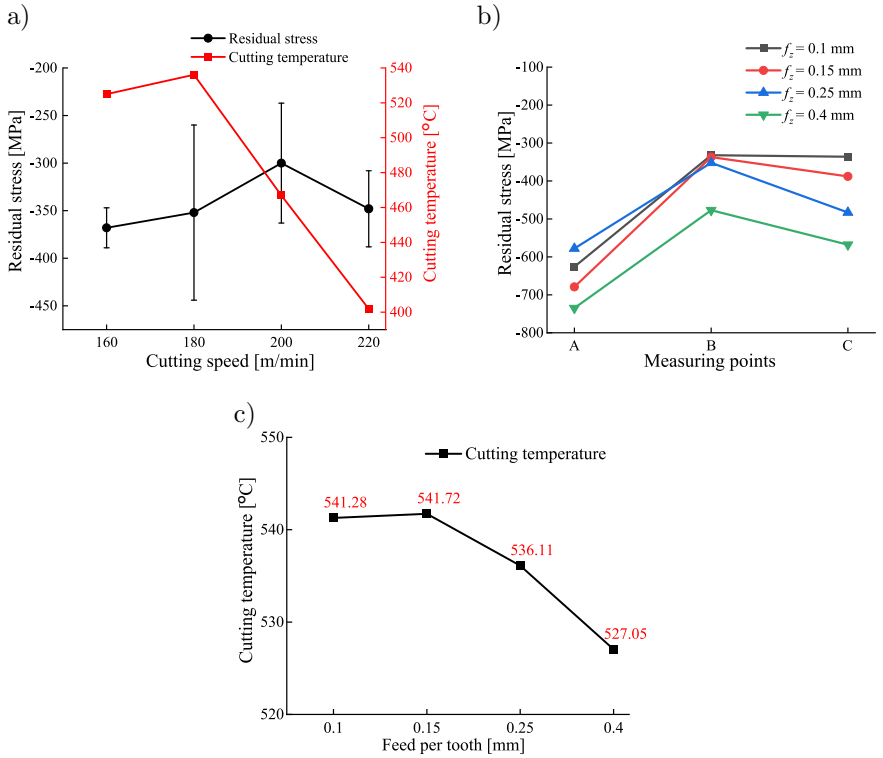

FIG. 7. The effect of cutting parameters on residual surface stress: a) effect of cutting speed on residual stress (tool #2, $f_z = 0.25$ mm, point B), b) residual stress at points located in the screw fragment (tool #2, $V_c = 180$ m/min), c) cutting temperature dependent on feed per tooth (tool #2, $V_c = 180$ m/min).

is 300 MPa. As the cutting speed increases, the cutting force tends to decrease (Fig. 6), so the tool's squeezing effect on the workpiece's surface is weakened, reducing the residual compressive stress on the surface. When the cutting speed is 160 m/min and 180 m/min, the cutting force is close and the surface residual stress reduction is insignificant. When the cutting speed increased to 200 m/min, the cutting force decreased considerably, and the surface residual compressive stress decreased more. The residual surface stress increases when the cutting speed increases to 220 m/min. This is because when the cutting speed is too high, although the cutting force decreases slightly compared with 200 m/min, the effect of reducing the surface residual compressive stress caused by thermal stress is weakened due to the considerable reduction in cutting temperature.

Figure 7b shows the variation of residual surface stress with the feed per tooth. The surface residual compressive stress tends to increase with the increase of feed per tooth ($V_c = 180$ m/min). The residual surface stress increase is insignificant when the feed per tooth varies between 0.1 mm and 0.25 mm, and increases significantly when the feed per tooth is 0.4 mm. Due to the increase of feed per tooth, the material removal rate becomes larger, which increases the deformation resistance of the cutting layer, and the growth of cutting force leads to the enhancement of the squeezing effect and the increase of residual stress on the workpiece surface. At the same time, the increase of feed per tooth has little impact on the change of cutting temperature, the evolution of residual surface stress caused by thermal stress is not apparent, and mechanical stress plays a dominant role in the change of residual stress. Under different feeding conditions, the residual compressive stress in the middle of the raceway is the smallest, the residual compressive stress on both sides is larger than that in the middle, and the residual compressive stress at point A in the direction of feed is the largest. It indicates that hard whirling is a gradual envelope forming process, and the tool's action time on both sides of the raceway is longer than that on the middle of the raceway. The tool's squeezing effect on both sides of the raceway surface is greater than that on the middle. And due to axial feed, the residual stress on the raceway surface along the feed direction shows a trend of first decreasing and then increasing.

Figure 8a shows that the surface roughness Ra of the raceway increases as the feed per tooth increases. The maximum Ra value of 0.31 μm occurs at the left position when feed per tooth is 0.4 mm. It indicates that when large feed is used, the surface quality is further reduced due to the increased height of the residual zone and the increased plastic deformation. When the feed per tooth increases from 0.15 mm to 0.25 mm, the surface roughness change is not apparent, and the Ra at the middle and right side changed from 0.17 μm to 0.16 μm, a slight decrease. With the increased cutting speed, the surface roughness of the raceway shows a wave-like change, but the difference is not significant. PCBN

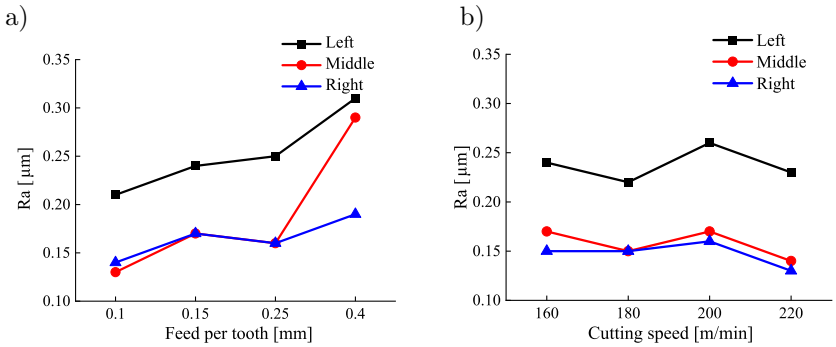

FIG. 8. The effect of cutting parameters on surface roughness: a) tool #4, $V_c = 160$ m/min, b) tool #3, $f_z = 0.25$ mm.

tools have low friction coefficient and anti-adhesion properties, which is not easy to form a retention layer and built-up edge on the tool's surface, so the effect of cutting speed on surface roughness is weak. When the cutting speed increases from 160 m/min to 180 m/min, the cutting force decreases as the cutting speed increases and the tool-chip friction decreases. There is a decreasing trend in Ra, where Ra at the left side is reduced from 0.24 μm to 0.22 μm. When the cutting speed is 200 m/min, the surface roughness increases instead of decreasing, although the cutting force decreases. When the cutting speed increases to 220 m/min, the cutting force decreases, which makes the surface roughness of the machining trend down again, reduced by about 0.03 μm. Along the feed direction, the surface roughness of the raceway decreases gradually. The surface roughness of the left section of the raceway in the backward feeding direction is the largest, the middle position is lower than that of the left surface, and the surface roughness of the right section is the lowest. It is mainly since the tool's squeezing effect on the workpiece surface gradually decreases from the forward feeding direction to the backward feeding direction during axial feeding. The tool can press the residual area of the protruding machined surface into the workpiece body, which is conducive to improving the surface quality.

3.2. Effect of tool edge geometry on cutting forces and surface quality

After preparation, the cutting edge of the hard whirling tool has a combination of negative chamfering and transition arc. Figure 9 shows the effect of tool parameters on cutting forces and surface quality in hard whirling at a cutting speed of 180 m/min and 0.25 mm per tooth feed (typical cutting conditions used for actual machining). It can be seen that when the chamfering edge is small (the chamfering edge length is 0.1 mm, and the chamfering edge angle is 20°), the cutting force first increases and then decreases as the tool edge radius in-

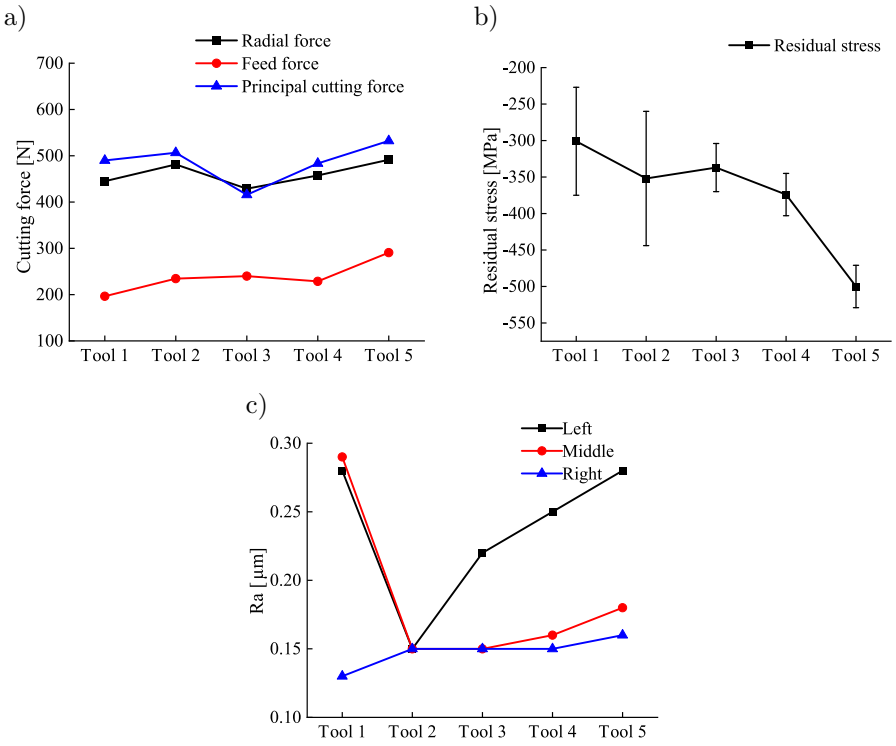

FIG. 9. The effect of tool parameters on: a) cutting forces, b) residual stress, c) surface quality.

creases from 10 μm to 30 μm. With the rise in the edge radius (from 10 μm to 20 μm), the tool becomes blunt, the squeezing effect of the edge on the workpiece becomes larger, the cutting deformation increases, and the cutting force increases. As the cutting edge radius increases to 30 μm, the interaction between the tool edge, the workpiece, and the chip is enhanced. The cutting temperature increases significantly, making the softened workpiece easier to cut and the cutting force decreases. When the chamfer is larger (chamfer length 0.15 mm, chamfer angle 25°), the cutting force increases more when the radius of the edge arc increases from 10 μm to 30 μm. It reflects that as the size of the chamfer increases, the pushing and squeezing effect of the tool on the workpiece becomes more and more considerable, further increasing the plastic deformation. From the comparison of tool 4 and tool 5, it can be seen that the three components of the cutting force become more significant with the increase of the chamfer size at the larger radius. The increase in chamfer size increases the workpiece deformation, while the growth of the heat dissipation area weakens the softening effect of the workpiece, and the cutting force increases significantly.

The residual compressive stress on the workpiece surface tends to increase with the tool edge radius. When the chamfer size is 0.1 mm × 20° and the tool

edge radius increases from 10 μm to 20 μm and 30 μm, the residual compressive stress on the workpiece surface increases by 18.6% and 24.3%, respectively. It may be due to the increase of the cutting edge radius to blunt the tool, increase the deformation of the cutting area, and further increase the residual stress by the violent squeezing effect of the flank face on the workpiece surface. When the tool edge radius is 30 μm, the increase of cutting temperature has a certain weakening effect on the residual stress, so the increase of surface residual compressive stress slows down. When the tool edge radius is the same, the workpiece surface's residual compressive stress increases with the negative chamfer size. The residual stress on the workpiece surface rises by 33.7% with tool 5 compared to tool 4. The possible reason is that increasing the negative chamfer's size intensifies the tool's pushing effect on the workpiece.

The surface roughness of the right section of the raceway changes gently, and the changes in the tool edge radius and chamfering parameters have little effect on the surface roughness of the right raceway area. When the chamfer size is 0.1 mm $\times$ 20°, in the left and middle sections of the raceway, the surface roughness decreases and then increases with the tool edge radius. The edge radius of tool 1 is 10 μm, and the relatively sharp edge is mainly shearing to the workpiece, and the extrusion effect on the machined surface is weak, resulting in low surface quality. In addition, the sharp edge strength is lower, and the tool defects may not be removed entirely because of lighter preparation. The edge is prone to early breakage, making the surface roughness larger. With the increased cutting edge radius, the pushing and ironing effect of the cutting edge on the machined surface increases, and the surface roughness decreases significantly. When the cutting edge radius is further increased to 30 μm, the tool becomes blunter, the plastic deformation in the cutting area increases, and the surface quality decreases. On the other hand, due to the minimum cutting thickness, when the edge radius is too large, part of the workpiece material on the machining surface will not be removed, increasing surface roughness. When a small edge radius (10 μm) is used, increasing the size of the chamfering will increase the edge strength and help reduce the surface roughness of the raceway. In the case of a large edge radius (30 μm), increasing the chamfer size increases the cutting force, and the machined surface roughness tends to increase.

3.3. Effect of edge radius on tool wear

In this paper, the tool wear is characterized by the maximum wear at the middle of the flank face. As shown in Fig. 10, the slope of the wear curve at the beginning of cutting is more significant and wears faster; after the cutting length of about 50 m, the tool wear slows down; after the cutting length of about 150 m, the tool wear increases sharply. The tool wear gradually increases as the

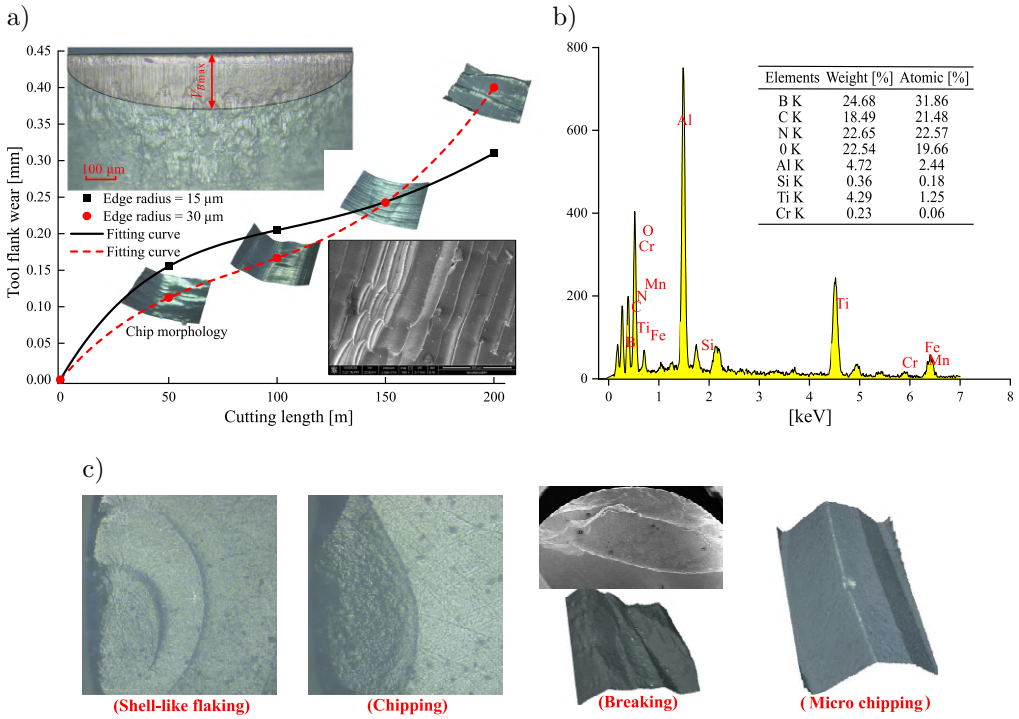

FIG. 10. Analysis of tool failure mechanism: a) tool flank wear curve, b) EDS analysis of tool's flank face, c) other forms of tool failure in hard whirling.

cutting progresses, the interaction between the tool and the chip is enhanced, and the chip deformation intensifies. When the cutting length is 150 m, the chip appears to have more considerable periodic undulation, and when the cutting length is 200 m, the chip deformation is more serious, reflecting the increased tool wear at this time. Combined with the test site state and chip morphology, it is believed that the tool flank wear is severe when the tool cuts to 150 m, and the approximate value of the tool flank wear at this time can be used as the tool wear standard.

In the early cutting stage, the tool wear with a small radius edge is larger than that with a large radius edge. With the cutting process, the microscopic defects on the surface layer of the small radius edge are gradually ground away, the edge quality has improved and the wear rate tends to level off. In the later cutting stage, the cutting edge quality becomes stable. As the sharpness of the small radius cutting edge is better than that of the large radius cutting edge, the interaction between the cutting edge and the workpiece is weaker than the large radius edge. Smaller cutting deformation results in less cutting force and cutting temperature, and the friction between the tool and the part also becomes

smaller. At this time, the flank wear rate of the tool with a large radius edge is faster than that of the tool with a small radius edge, and the wear exceeds that of the tool with a small edge radius. From the perspective of ensuring the machining quality and prolonging the tool life, the large radius tool should be resharpened when the tool is close to the wear standard.

As shown in Fig. 10b, some chemical elements on the flank face are not inherent to the tool. These elements are mainly derived from the workpiece. More oxygen element on the flank face indicates a significant oxidation reaction. The EDS analysis shows that the flank face wear is primarily due to oxidation and adhesive wear. In addition, the flank face wear gradually decreases from the middle position to the left and right sides. It was also found that 80% of the tools with an edge radius of 15 μm had different degrees of chipping, flaking and breaking, while only 20% of the tools with an edge radius of 30 μm had early breaking and 20% had late fatigue flaking. It can be concluded that increasing the edge preparation radius within a specific range can improve the edge strength and reduce the probability of early tool breakage. Under the priority conditions, a relatively large edge radius and timely sharpening should be used to extend tool life and ensure the machining quality of the screw raceway.

4. Conclusions

1) The proposed toolholder-type cutting force measurement device is suitable for hard whirling and can obtain cutting force signals effectively. The cutting force increases with the increase of feed per tooth and cutting speed has little effect on cutting force. When the cutting speed was 160 m/min and the feed per tooth was increased from 0.1 mm to 0.4 mm, the mean values of radial force, feed force and principal cutting force increased to 68.37%, 43.76%, and 126.63%, respectively. The residual compressive stress on the raceway surface favors improving its service performance. With the increase of feed per tooth, the surface residual stress and roughness tend to increase. With the increase in cutting speed, the workpiece's residual surface stress decreases and then increases. At a cutting speed of 160 m/min, the residual surface compressive stress on the screw is 368 MPa. In machining, the surface quality and machining efficiency should be considered, and medium and low range feeds and higher cutting speed should be employed as much as possible.
2) Increasing the chamfer increases the cutting force significantly. The residual compressive stress on the workpiece surface tends to increase with the edge radius and chamfer increase. When the edge radius is 10 μm, increasing the chamfer is beneficial to reduce the surface roughness; in the case of a large edge radius (30 μm), the surface roughness increases when the

chamfer size is increased. In hard whirling, try to choose a smaller combination of edge radius and chamfering parameters while ensuring the edge strength.

3) There are differences in the surface quality of the raceway at each position after machining, and the residual stress on the raceway surface along the feed direction shows a trend of first decreasing and then increasing. The surface roughness of the raceway on the side facing the feed direction changes gently with the change of feed per tooth and cutting speed, and the surface quality of the raceway is stable.
4) The tool flank wear in hard whirling follows the conventional tool wear law. On the premise that the tool has no early brittle damage, the tool flank wear when the cutting length is 150 m can be used as the tool wear standard. The initial wear of a tool with a 30 μm edge radius is less than that of a tool with a 15 μm edge radius, but the wear of a tool with a 30 μm edge radius increases faster in the later stages of cutting. From the perspective of ensuring the processing quality and prolonging the tool's service life, when the tool is close to the wear standard, the tool with a large cutting edge radius should be resharpened in time.

Acknowledgments

The study was funded by the National Natural Science Foundation of China (No. 51605414), the Postgraduate Research and Practice Innovation Project of Yancheng Institute of Technology (SJCX21_XZ004, SJCX22_XZ017, SJCX22_XY 034), and the Key Laboratory Fund Project of Zhejiang Provincial Key Laboratory for Cutting Tools (ZD202110). The authors extend their gratitude to the funding bodies for supporting this work.

References

1. Matsumura T., Serizawa M., Ogawa T., Sasaki M., Surface dimple machining in whirling, *Journal of Manufacturing Systems*, **37**(2): 487–493, 2015, doi: 10.1016/j.jmsy.2014.07.008.
2. Kennedy B., Whirled piece, *Cutting Tool Engineering Magazine*, **57**(4): 28–34, 2005.
3. Son J.H., Han C.W., Kim S.I., Jung H.C., Lee Y.M., Cutting forces analysis in whirling process, *International Journal of Modern Physics B*, **24**(15–16): 2786–2791, 2010, doi: 10.1142/S0217979210065635.
4. Lee M.H., Kang D.B., Son S.M., Ahn J.H., Investigation of cutting characteristics for worm machining on automatic lathe – Comparison of planetary milling and side milling, *Journal of Mechanical Science and Technology*, **22**(12): 2454–2463, 2008, doi: 10.1007/s12206-008-0713-1.

5. Liu C., He Y., Wang Y.L., Li Y., Wang S., Wang L., Wang Y., An investigation of surface topography and workpiece temperature in whirling milling machining, *International Journal of Mechanical Sciences*, **164**: 105182, 2019, doi: 10.1016/j.ijmecsci.2019.105182.

6. He Y., Liu C., Wang Y.L., Li Y., Wang S., Wang L., Wang Y., Analytical modeling of temperature distribution in lead-screw whirling milling considering the transient undeformed chip geometry, *International Journal of Mechanical Sciences*, **157–158**: 619–632, 2019, doi: 10.1016/j.ijmecsci.2019.05.008.

7. Guo Q., Chang L., Ye L., Wang Y., Feng H., Cao Y., Lian Q., Li Y., Residual stress, nanohardness, and microstructure changes in whirlwind milling of GCr15 steel, *Materials and Manufacturing Processes*, **28**(10): 1047–1052, 2013, doi: 10.1080/10426914.2013.763963.

8. Guo Q., Ye L., Wang Y.L., Feng H., Li Y., Comparative assessment of surface roughness and microstructure produced in whirlwind milling of earing steel, *Machining Science and Technology*, **18**(2): 251–276, 2014, doi: 10.1080/10910344.2014.897843.

9. Liu C., He Y., Li Y.F., Wang Y., Wang S., Wang Y., Modeling of residual stresses by correlating surface topography in machining of AISI 52100 steel, *Journal of Manufacturing Science and Engineering*, **144**(5): 051008, 2022, doi: 10.1115/1.4052706.

10. Guo Q., Wang M.L., Xu Y.F., Wang Y., Minimization of surface roughness and tangential cutting force in whirlwind milling of a large screw, *Measurement*, **152**(3): 107256, 2019, doi: 10.1016/j.measurement.2019.107256.

11. Liu C., He Y., Li Y.F., Wang Y., Wang L., Wang S., Wang Y., Predicting residual properties of ball screw raceway in whirling milling based on machine learning, *Measurement: Journal of the International Measurement Confederation*, **173**: 108605, 2020, doi: 10.1016/j.measurement.2020.108605.

12. Wang Y.L., Yin C., Li L., Zha W., Pu X., Wang Y., Wang J., He Y., Modeling and optimization of dynamic performances of large-scale lead screws whirl milling with multipoint variable constraints, *Journal of Materials Processing Technology*, **276**(1): 116392, 2019, doi: 10.1016/j.jmatprotec.2019.116392.

13. He Y., Wang L.X., Wang Y.L., Li Y., Wang S, Wang Y., Liu C., Hao C., An analytical model for predicting specific cutting energy in whirling milling process, *Journal of Cleaner Production*, **240**: 118181, 2019, doi: 10.1016/j.jclepro.2019.118181.

14. Zhu H.Y., Ni S.Y., Li Y., Experimental study and design for PCBN tools used in large-scale thread hard whirling, *Manufacturing Technology & Machine Tool*, (6): 93–95, 2014.

15. Denkena B., Biermann D., Cutting edge geometries, *CIRP Annals – Manufacturing Technology*, **63**(2): 631–653, 2014, doi: 10.1016/j.cirp.2014.05.009.

16. Wu X., Li L., He N., Yao C., Zhao M., Influence of the cutting edge radius and the material grain size on the cutting force in micro cutting, *Precision Engineering*, **45**: 359–364, 2016, doi: 10.1016/j.precisioneng.2016.03.012.

17. Ventura C.E.H., Chaves H.S., Campos Rubio J.C., Abrão A.M., Denkena B., Breidenstein B., The influence of the cutting tool microgeometry on the machinability of hardened AISI 4140 steel, *The International Journal of Advanced Manufacturing Technology*, **90**(9): 2557–2565, 2017, doi: 10.1007/s00170-016-9582-4.

18. Klocke F., Kratz H., Advanced tool edge geometry for high precision hard turning, *CIRP Annals – Manufacturing Technology*, **54**(1): 47–50, 2005, doi: 10.1016/S0007-8506(07)60046-8.

19. Rech J., Yen Y.C., Schaff M.J., Hamdi H., Altan T., Bouzakis K.D., Influence of cutting edge radius on the wear resistance of PM-HSS milling inserts, *Wear*, **259**(7–12): 1168–1176, 2005, doi: 10.1016/j.wear.2005.02.072.

20. Endres W.J., Kountanya R.K., The effects of corner radius and edge radius on tool flank wear, *Journal of Manufacturing Processes*, **4**(2): 89–96, 2002, doi: 10.1016/S1526-6125(02)70135-7.

21. Kang Z., *Experimental research on turning process and surface integrity with minimum quantity lubrication* [in Chinese], PhD thesis, Shanghai Jiao Tong University, 2011.

22. Qian L., Hossan M.R., Effect on cutting force in turning hardened tool steels with cubic boron nitride inserts, *Journal of Materials Processing Technology*, **191**(1–3): 274–278, 2007, doi: 10.1016/j.jmatprotec.2007.03.022.

23. Chen R.Y., *Metal Cutting Principle*, 2nd ed., Machinery Industry Press, 2002.

24. Ozlu E., Budak E., Molinari A., Analytical and experimental investigation of rake contact and friction behavior in metal cutting, *International Journal of Machine Tools & Manufacture*, **49**(11): 865–875, 2009, doi: 10.1016/j.ijmachtools.2009.05.005.

Received October 12, 2022; accepted version March 15, 2023.